

AD-A094 119

AIR FORCE GEOPHYSICS LAB HANSCOM AFB MA

F/G 4/2

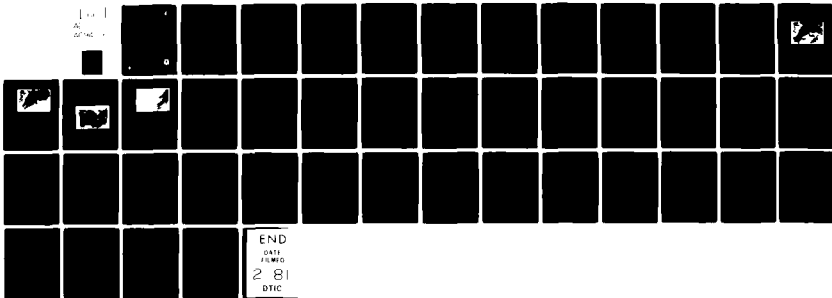
TESTS OF SPECTRAL CLOUD CLASSIFICATION USING DMSP FINE MODE SAT--ETC(U)

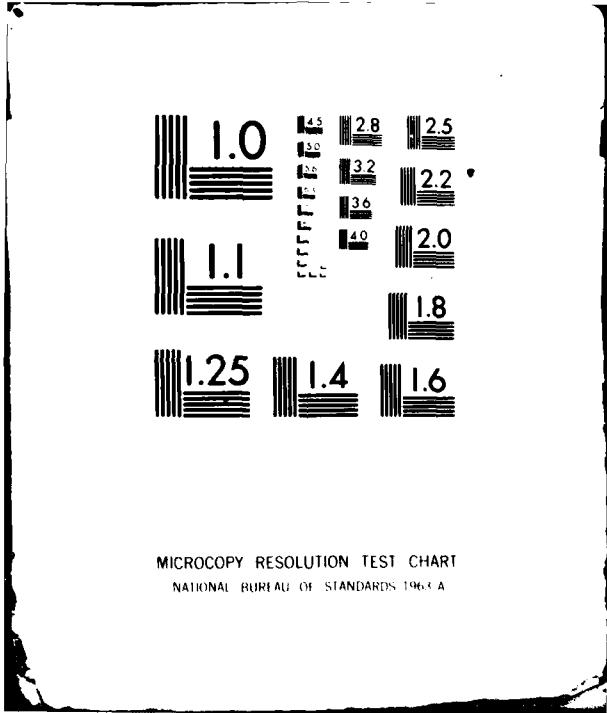
JUN 80 J T BUNTING, R F FOURNIER

UNCLASSIFIED

AFGL-TR-80-0181

NL





AD A094119

**Tests of Special Cloud Characteristics
Using DMSP Fine Mode Scatter Data**

**JAMES T. BUNTING
RONALD F. FOURNIER**

2 June 1980

Approved for public release; distribution unlimited.

**METEOROLOGY DIVISION PROJECT 4471
AIR FORCE GEOPHYSICS LABORATORY
HANCOM AFB, MASSACHUSETTS 01930**

AIR FORCE SYSTEMS COMMAND 4471

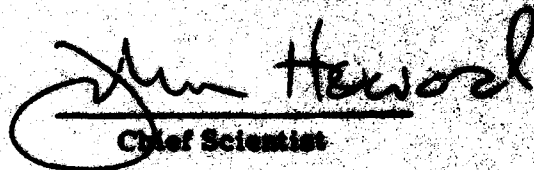
FILE COPY

SP-115
11/1/80

This report has been reviewed by the RSD Information Office and is
releasable to the National Technical Information Service.

This technical report has been reviewed and
is approved for publication.

FOR THE COMMANDER


Chief Scientist

Qualified requestors may obtain additional copies from the
Defense Technical Information Center. All others should apply to the
National Technical Information Service.

Unclassified

SECURITY CLASSIFICATION OF THIS PAGE (When Data Entered)

REPORT DOCUMENTATION PAGE		READ INSTRUCTIONS BEFORE COMPLETING FORM
1. REPORT NUMBER 14 AFGL-TR-88-0181	2. GOVT ACCESSION NO. AD-A094 119	3. RECIPIENT'S CATALOG NUMBER
4. TITLE (and Subtitle) 6 TESTS OF SPECTRAL CLOUD CLASSIFICATION USING DMSP FINE MODE SATELLITE DATA	5. TYPE OF REPORT & PERIOD COVERED Scientific, Interim.	
7. AUTHOR(s) 10 James T. Bunting Ronald F. Fournier	6. PERFORMING ORG. REPORT NUMBER ERP No. 704 ✓	
9. PERFORMING ORGANIZATION NAME AND ADDRESS Air Force Geophysics Laboratory (LYU) ✓ Hanscom AFB Massachusetts 01731	10. PROGRAM ELEMENT, PROJECT, TASK AREA & WORK UNIT NUMBERS 62101F 17 / 17 6670801	
11. CONTROLLING OFFICE NAME AND ADDRESS Air Force Geophysics Laboratory (LYU) Hanscom AFB Massachusetts 01731	12. REPORT DATE 11 2 Jun 1988	
14. MONITORING AGENCY NAME & ADDRESS (if different from Controlling Office) 9 Environmental research group	13. NUMBER OF PAGES 42 12 / 44	
	15. SECURITY CLASS. (of this report) Unclassified	
15a. DECLASSIFICATION DOWNGRADING SCHEDULE		
16. DISTRIBUTION STATEMENT (of this Report) Approved for public release; distribution unlimited.		
17. DISTRIBUTION STATEMENT (of the abstract entered in Block 20, if different from Report)		
18. SUPPLEMENTARY NOTES		
19. KEY WORDS (Continue on reverse side if necessary and identify by block number) Infrared sensors Fourier transform Visible sensors Satellite imagery Cloud types Satellite data processing Cloud categories High resolution imagery Weather satellites		
20. ABSTRACT (Continue on reverse side if necessary and identify by block number) → A computer-based processor for satellite imagery was tested on samples of DMSP visible and IR imagery data smoothed to 0.6 n mi resolution. The data were displayed on the AFGL Man-computer Interactive Data Access System so that meteorologists could label small areas (25 X 25 n mi) with one of nine possible cloud categories from the AF 3D Nephanalysis Program (3DNEPH). The computer-based processor labeled the same areas by computing a two-dimensional fast Fourier transform (FFT) and comparing the results to average wavenumber spectra for the cloud categories. Classification		

DD FORM 1 JAN 73 1473 EDITION OF 1 NOV 65 IS OBSOLETE

Unclassified

SECURITY CLASSIFICATION OF THIS PAGE (When Data Entered)

409578

not

Unclassified

SECURITY CLASSIFICATION OF THIS PAGE (When Data Entered)

20. (Cont)

→ accuracies were 65% for visible, 65% for IR and 81% for combined data. The classification accuracies were appreciably better than chance and a simplified processor which used only the averaged values of satellite data over an area. Accuracies improved if some categories were merged.

The results were also compared to a cloud typing procedure in the 3DNEPH and to some earlier studies. The results were generally good for categories with small-scale cloud features such as cumulus or cirrus clouds, but the overall accuracy of classification for all cloud categories was not significantly better than verifications cited in earlier studies.

Two potential refinements to the spectral processors, namely, removing the effects of backgrounds such as land, water, and snow cover and minimizing sensitivity to varying fractional cloud cover from case to case, are also discussed.

A

Unclassified

SECURITY CLASSIFICATION OF THIS PAGE (When Data Entered)



A

Contents

1. INTRODUCTION	5
2. OTHER STUDIES	7
3. DMSP FINE MODE DATA	8
4. SUBJECTIVE CLOUD CLASSIFICATION	11
5. AUTOMATED CLOUD CLASSIFICATION	15
6. RESULTS OF THE STUDY	18
6.1 Mean Spectra of Cloud Types	19
6.2 Autocorrelation of Picture Elements	22
6.3 Classification by Mean Values	25
6.4 Classification for Nine Cloud Types	27
6.5 Detection of Small-Scale Cloud Features	29
6.6 Comparison to 3DNEPH	30
6.7 Multilayered Clouds and Merged Categories	33
6.8 Adjustments for Varying Backgrounds	34
6.9 Visible and IR Covariance Consideration	36
7. CONCLUSIONS	36
REFERENCES	39
APPENDIX A: Implications of Changing the Resolution of Satellite Data	41

Illustrations

1. Photograph of the AFGL McIDAS CRT Showing DMSP Visible Data	10
2. Photograph of Same Area Shown in Figure 1 As Viewed by the IR Sensor (8 to 13 μm)	11
3. DMSP Visible Data at 0.6 n mi Resolution Over Egypt and the Mediterranean Sea (upper right)	12
4. Photograph of Same Area Shown in Figure 3 as Viewed by the IR Sensor	13
5. Mean Visible Spectra For Four of the Nine Cloud Categories of the 3DNEPH	20
6. Mean IR Spectra For Four of the Nine Cloud Categories of the 3DNEPH	20
7. Mean Visible Spectra For the Remaining Five Cloud Categories of the 3DNEPH	21
8. Mean IR Spectra For the Remaining Five Cloud Categories of the 3DNEPH	21
9. The Autocorrelation Function For Three Cases of Visible Data	23
10. The Autocorrelation Function For Three Cases of IR Data	24
11. Mean IR and Visible Values For the Nine Cloud Categories	26

Tables

1. Cloud Type Categories From 3DNEPH	14
2a. Autocorrelation Parameters For Visible Data	24
2b. Autocorrelation Parameters For IR Data	25
3. Classification Accuracy For Two Data Sets	27
4. Classification Accuracy For Nine Categories	28
5. Numerical Values of Probability Terms For Nine Cloud Types in Subset 1	29
6. A Comparison of Observed Cloud Types to Automated Classifications	30
7. Classification Accuracy For 3DNEPH Categories	32
8. Cloud Categories Used in Cloud Classification Studies	34
9. Classification Accuracy For Five Categories: (Sc/St/Cu), (Ci/Cs), Cb, Clear	35

Tests of Spectral Cloud Classification Using DMSP Fine Mode Satellite Data

1. INTRODUCTION

Operational satellite imagers are now capable of ground resolution of less than 1 n mi for both visible and IR channels. Photocopy or TV displays of such imagery reveal a wealth of detail including such features as small-scale cumulus, cirro-cumulus, or wave clouds. Meteorologists looking at the images can readily identify these features and use this information to support highly important Air Force projects. It is also apparent to the meteorologists that the small-scale features are often not resolved in the currently operational cloud analysis program (3DNEPH)^{1, 2} that uses satellite data with a ground resolution of approximately 3 n mi. For example, when individual cumulus clouds are not resolved in the 3 n mi data, the satellite data processor might incorrectly classify the cloudy area as either clear or low overcast depending on the extent of coverage by the cumulus clouds. Either misclassification could have grave consequences if used to support weapons systems such as Precision Guided Munitions (PGMs) since these tend to be sensitive to the cloud cover at low altitudes. Moreover, cumulus clouds often grow during the day so a misclassification of clear could also lead to a bad forecast.

(Received for publication 30 May 1980)

1. Fye, F. K. (1978) The AFGWC Automated Cloud Analysis Model, AFGWC Technical Memorandum 78-002.
2. Coburn, A. R. (1971) Improved Three-Dimensional Nephanalysis, AFGWC Technical Memorandum 71-2.

Given DoD requirements for cloud analysis, and the limited time and manpower for human interpretation of photocopy, there has been strong impetus to automate the processing of very high resolution data. Automation has not been achieved thus far due to the massive quantities of data involved. Moreover, spacecraft can presently store and transmit only limited quantities of fine mode imagery so that coverage is poor on many orbits. Consequently, automated procedures that are computationally fast and efficient or are suitable for use onboard the satellite are of particular value.

This report summarizes tests of a computer-based processor to classify cloud types using fine mode data* from the Defense Meteorological Satellite Program (DMSP). Earlier studies sponsored by the Air Force Geophysics Laboratory (AFGL) have considered requirements for cloud analysis and developed the procedure tested here. Pickett and Blackman³ surveyed processing of satellite imagery at the Air Force Global Weather Central (AFGWC) to identify automated imagery processing techniques of potential value. Fourier spectral analysis was identified as the most promising technique to upgrade automated processing of weather satellite imagery. Initial demonstrations of spectral analysis using a two-dimensional Fast Fourier Transform (FFT) over selected cloudy regions were given by Blackman and Pickett⁴ and by Fournier.⁵ A test of a spectral classifier was described by Pickett and Blackman.⁶ The test used visible data from DMSP Block 5C satellites with cloud type verification provided by satellite meteorologists who viewed displays of the imagery data on a TV screen. While automated classifications using visible data were found to be appreciably better than chance (46% correct classifications for the automated program vs 17% for chance), the performance of 46% was less than expected. On the other hand, it was observed that many of the misclassifications were reasonably close to correct, for example, classifying cumulus as strato-cumulus or cirrostratus as cirrus.

*The term fine mode data refers to both visible (0.4 - 1.1 μm) and IR (8 - 13 μm) measurements by the Operational Linescan System on DMSP Block 5D spacecraft. The nominal resolution of these measurements on the Earth's surface is 0.3 n mi.

3. Pickett, R. M., and Blackman, E. S. (1976) Automated Processing of Satellite Imagery Data at Air Force Global Weather Central, BBN No. 3275, Interim Report. F19628-76-C-0124, Bolt Beranek and Newman Inc., Cambridge, MA 02138.
4. Blackman, E. S., and Pickett, R. M. (1977) Automated Processing of Satellite Imagery Data at the Air Force Global Weather Central: Demonstrations of Spectral Analysis, AFGL-TR-77-0080, AD A039918.
5. Fournier, R. F. (1977) An Initial Study of Power Spectra for Satellite Imagery, AFGL-TR-77-0295, AD A058483.
6. Pickett, R. M., and Blackman, E. S. (1979) Automated Processing of Satellite Imagery Data: Test of a Spectral Classifier, AFGL-TR-79-0040, AD A068663.

A different approach to the same requirements was taken by Hawkins.⁷ A bit reduction algorithm was described which is capable of reducing the total number of bits in a DMSP image by a factor of 6 while maintaining most of the image integrity.

This report extends previous studies since multispectral images of both IR and visible data from a Block 5D satellite are subjected to spectral analysis and cloud classification using a straightforward extension of the computational procedure and a similar set of cloud cases selected by satellite meteorologists. The following sections describe related literature, DMSP data, subjective and automatic classification of the data, and our conclusions. Properties of the FFT, classification logic, and computer applications are described in a separate report by d'Entremont⁸ and will not be repeated here except as needed for clarity. The report does give, however, a complete discussion of the results of automated classification experiments.

2. OTHER STUDIES

Both before and during the AFGL studies, other investigators have conducted similar studies. Since these studies are independent of our own by virtue of their use of different data sets, satellites, cloud truth verification, and computer codes they serve to substantiate our conclusions on the strengths and weaknesses of automated cloud classification. In 1963, Leese and Epstein⁹ applied two-dimensional spectral analysis to manually-digitized TIROS photographs. They used the spectral analysis to quantify patterns of cloud lines and cells with horizontal dimensions in the range of 20 to 100 miles. Darling and Joseph¹⁰ applied several decision algorithms to classify noncumulus, cumulus with polygonal cells, and cumulus with solid cells from NIMBUS I cloud pictures. In a comprehensive study, Booth¹¹ used both visible and IR NOAA 1 data to classify up to six cloud categories. The spectral energies at various wavenumbers were included as predictors. The mean spatial resolution of satellite measurements was given as 6 n mi, so that some consideration of the implications of this size difference is necessary before transferring his results to fine mode satellite data. Sikula¹² made the first application of spectral analysis to DMSP data. Very high resolution (0.33 n mi) visual data were analyzed by a two-dimensional FFT. He also demonstrated that cumulus and cirrus clouds had substantially different spectral signatures and that a data compression of about 100 to 1 could be achieved by using sums of spectral coefficients. Parikh^{13, 14} reported on a comparative study of cloud classification techniques using NOAA 1 data and later did an evaluation of the techniques using data from the geostationary satellite SMS 1. She considered both four and three categories of cloud conditions.

(Due to the large number of references cited above, they will not be listed here. See References, page 39.)

Moreover, instead of using a transform to quantify the variability within arrays of satellite data she defined other parameters called "textural features". Harris and Barrett,¹⁵ apparently unaware of the 3DNEPH program, proposed an objective procedure to distinguish three cloud types using measurements taken from a DMSP visible transparency which they scanned by microdensitometer. In summary, although a variety of cloud categories were used by the various authors, accuracies of classification were moderately good, with higher accuracy when cloud types are grouped into broader categories.

Aside from applications to cloud classification, a considerable literature exists for spectral analysis of images of the oceans, earth resources, and so on. It is beyond the scope of this report to survey this literature. However, a good introduction is provided by Steiner and Salerno in the Manual of Remote Sensing.¹⁶ The mathematical background is treated in depth by Duda and Hart.¹⁷

3. DMSP FINE MODE DATA

The DMSP Block 5D spacecraft and Operational Linescan System (OLS) sensors have been described by Nichols et al¹⁸ and by Spangler.¹⁹ The spacecraft are in sun-synchronous polar orbits at 450 n mi altitudes. This study used data taken by Vehicle F-1 that has an ascending node near local noon. The OLS, which provides the fine mode imagery, has a visible daytime response from 0.4 to 1.1 μm and an IR response from 8 to 13 μm . The OLS is a scanning optical telescope system. An approximately constant ground resolution (within a factor of 2) is maintained by two special features of the OLS. First, the scanning optics are driven in a sinusoidal or back and forth motion rather than the conventional circular motion. Since the scanning velocity slows as the telescope approaches its limit of scan, a nearly constant sampling rate can be maintained along the scan line. Second, the system field of view is reduced as the telescope approaches its limit of scan by means of switching from three detector elements to one. The result is an approximate

15. Harris, R., and Barrett, E. C. (1978) Toward an objective nephanalysis, J. Appl. Meteor. 17:1258-1266.
16. Steiner, D., and Salerno, A. E. (1975) Remote sensor data systems, processing and management, Manual of Remote Sensing, Keuffel and Esser Co., pp 611-803.
17. Duda, R. O., and Hart, P. E. (1973) Pattern Classification and Scene Analysis, John Wiley and Sons.
18. Nichols, D. A. (1975) Block 5D Compilation, Defense Meteorological Satellite Program, Los Angeles AFS CA 90009.
19. Spangler, M. J. (1974) The DMSP primary data sensor in Proceedings of the 6th Conf. on Aerospace and Aeronautical Meteor. El Paso, TX, pp 150-157.

0.3 n mi resolution along scan lines. The frequency of oscillation of the scanning optics is sized to provide 0.3 n mi resolution across track, that is, between scan lines.

The approximately constant footprint size and equal spacing of OLS data on the earth are great advantages to spectral analysis or any other technique which extracts information before the data are earth-located. Applications of a two-dimensional FFT to arbitrary positions along a satellite data swath require approximately equal spacing of data elements and constant footprint size. The importance of these requirements can easily be shown by test patterns for the two-dimensional FFT. Most earlier studies had to restrict coverage or alter the data so that scale sizes did not depend on location along the scan line. For example, Pickett and Blackman⁶ used only areas reasonably close to the subtrack of the DMSP 5C satellites while Booth¹¹ repeated scan lines and stretched them near the limit of scan in order to yield approximately equal intervals between NOAA-1 data elements.

In late February 1978, a series of partial orbits of OLS data were saved by AFGWC. Both digital magnetic tapes and photocopies were provided to AFGL. The OLS sample included both fine mode visible (Light Fine, LF) and IR (Thermal Fine, TF) data. The tapes contained data in a 2×2 mode, which means that two adjacent data elements from two consecutive scan lines of the 0.3 n mi data were averaged to yield a nominal ground resolution of 0.6 n miles. The 2×2 averaged mode was provided since equipment limitations at AFGWC during early usage of the Block 5D system would not allow digitized data saves at full resolution without undue interruption of operations. This limitation has subsequently been removed.

Although our prime motivation was the detection of small-scale cloud elements in fine mode data, we believe that the 0.6 n mi data are adequate for demonstrating the feasibility of spectral analysis techniques and estimating the performance of an automated classifier for cloud types. This confidence is based on the related studies (discussed in Section 2) that used data from different satellites with various ground resolutions. Hence, in the remainder of this report, references to satellite data will always imply the 0.6 n mi data unless some other resolution is specified. Some other implications of substituting 0.6 for 0.3 n mi data will be discussed in Appendix A.

The partial orbits were always the R+9 orbit, that is, nine orbits after the reference orbit of the day. During the sunlit portion of this orbit, the spacecraft ascends over Africa, the Middle East, and Europe traveling from the southeast to the northwest. Examples are shown in Figures 1 and 2 that show part of orbit 7399+9 displayed on the AFGL Man-computer Interactive Data Access System (McIDAS). Figure 1 has visible data while Figure 2 has IR data. The McIDAS CRT

shows about 90% of the 1600 n mi swath width of data scans and was generated by displaying every fifth element of every fifth scan line. In the clearer areas on the lower part of Figure 1, portions of Libya, Egypt, the Sinai Peninsula, Saudi Arabia and the Persian Gulf can be seen. The landmarks are not prominent in the IR channel (Figure 2) due to greater atmospheric attenuation.

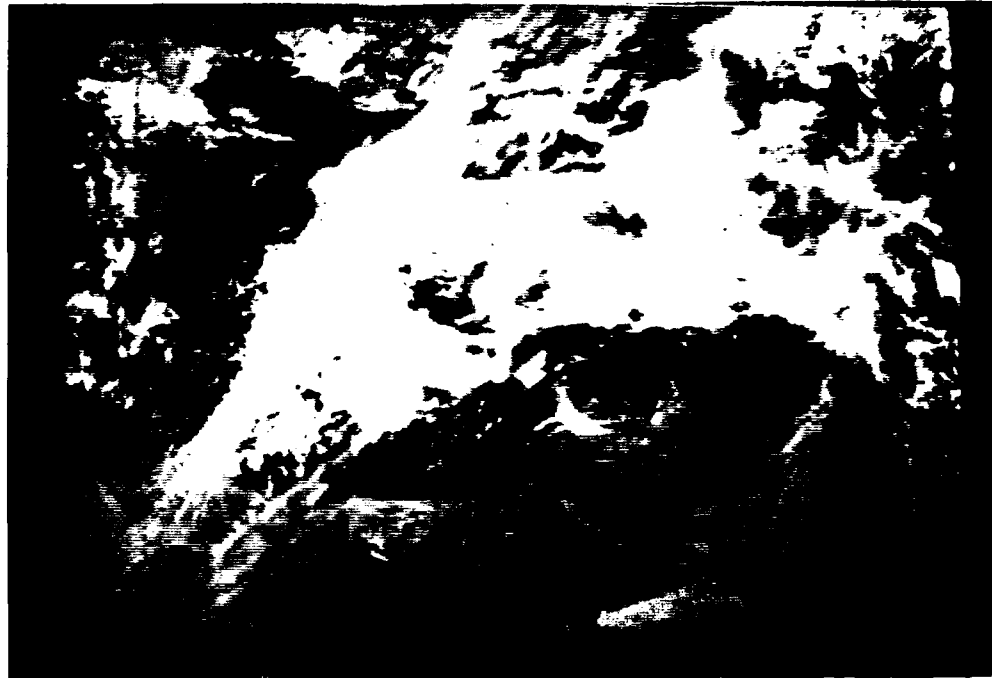


Figure 1. Photograph of the AFGL McIDAS CRT Showing DMSP Visible Data. The width of the picture shows about 90% of the range of data scans by the OLS instrument. Data were taken on 15 February 1978 by Block 5D vehicle F-1 over the Middle East. Africa and the Sinai Peninsula can be seen in the lower left and center of the picture. In this picture, as well as in Figure 2, image quality has been noticeably degraded since only every fifth element of every fifth scan line is displayed



Figure 2. Photograph of Same Area Shown in Figure 1 As Viewed By the IR Sensor (8 to 13 μm). Cold temperatures appear as bright tones while warm temperatures are dark

4. SUBJECTIVE CLOUD CLASSIFICATION

The development of the automated classifier requires a series of "cloud truth" cases. They were provided by subjective cloud classification obtained manually by examining images on the McIDAS. The OLS data tapes were converted from 6 bits to 8 bits per picture element that is required by the McIDAS. This change has a negligible impact on the picture quality. However, since all the data values are multiplied by 4, the subsequent calculations of spectra are changed.

Since the data were taken in February, there was considerable snow cover over Europe and Asia. In order to avoid ambiguity, we avoided snow covered areas. Therefore, the northern scan lines of the original tapes were not processed and the analysis was concentrated on Southern Europe, the Mediterranean, Africa, and the Middle East. Photographs such as Figures 3 and 4 were loaded into the McIDAS digital and video disks. These photographs displayed every scan line and

picture element of the 0.6 n mi data in an array of 500 lines by 672 picture elements, or about 300×400 n mi per image. Alphanumerics for identification were written on top of the frames. Small enhancements were given to both visible and IR gray scales to facilitate the picture interpretation.

McIDAS interactive graphics commands will display a cursor of arbitrary size on the CRT and move it anywhere with a joystick. A square cursor of 37×37 picture elements was used in the analysis since it encloses a ground area of 25×25 n mi that is the current unit of analysis for the 3DNEPH.¹ The array size is adjustable in the spectral analysis. For example, arrays of 75×75 were used with 0.3 n mi Block 5C visible. Once an array size is chosen, however, it must remain constant for the entire experiment which includes the cloud truth set and subsequent calculations.



Figure 3. DMSP Visible Data at 0.6 n mi Resolution Over Egypt and the Mediterranean Sea (upper right). This area appears in the lower left of Figure 1 and it is 1/25 of the area in Figure 1. Cirrus clouds appear on the right side of the picture. A small box (CRT cursor) in the lower half of the cloud area encloses 37×37 picture elements and covers an area of about 25×25 n mi on the earth's surface



Figure 4. Photograph of Same Area Shown in Figure 3 As Viewed By the IR Sensor. The cirrus clouds, which are not bright in the visible image, appear cold in this image

Nine classes of cloud conditions were sought. The classes, listed in Table 1, are the ones currently used in the 3DNEPH program. It should be noted that "clear" is included as a class and that only one mixed class (As/Ns) appears in the listing. Cloudy areas were assigned a class after a number of factors were considered. How bright and cold the clouds appeared was a factor, along with smooth vs rough texture, relative position in a circulation pattern such as a cyclonic storm, the sizes and shapes of individual clouds, and so on. The images were loaded into the McIDAS so that the operator could switch back and forth from visible to IR data. This procedure was found to be highly useful for separating low, middle, and high cloud types. The number of cases for each cloud type is given in Table 1. The satellite meteorologists who examined the images were free to select cloud truth samples anywhere, subject to the following constraints:

- (1) Areas of 37×37 picture elements with only one of the classes appearing in Table 1 were chosen,
- (2) Areas with snow cover were avoided,

- (3) Areas could have either a land or a water background so long as no coastline was included,
- (4) Areas over a coastline could be chosen if the cloud cover completely obscured the coastline,
- (5) Every effort was made to find some samples for all cloud categories even if it led to overrepresentation of the infrequently observed categories such as Ac,
- (6) Scan lines that appeared bad were not permitted to cross a sample area,
- (7) Overlapping of sample areas was avoided.

The selection of samples on the McIDAS was greatly aided by the MS command, which was written specifically for the use of this project. Once a suitable area had been found and the box-shaped cursor was placed over it, the 37×37 arrays of both visible and IR data could be transferred from the McIDAS digital disk onto a separate tape. The operator identified the cloud and background types in the MS command. Bookkeeping information such as the orbit number and line and element identification of the sample were automatically written on the tape along with the arrays. When a number of samples had been collected on tape, subjective classification was complete and the tape was used as input to the automated classification program.

Table 1. Cloud Type Categories From 3DNEPH

Type	Abbreviation	Number of Cases
Stratocumulus	Sc	7
Stratus	St	10
Cumulus	Cu	24
Alto cumulus	Ac	9
Altostratus/ Nimbostratus	As/Ns	5
Cirrus	Ci	36
Cirrostratus	Cs	19
Cumulonimbus	Cb	14
Clear	Clear	19

5. AUTOMATED CLOUD CLASSIFICATION

The mathematical basis and approximations of automated cloud classification have been described in past reports by Blackman and Pickett⁴ and by Fournier.⁵ The extension of the techniques to the IR and visible data saves from Block 5D Vehicle F-1 is described in a recent report by d'Entremont.⁸ A summary of the descriptions in these reports is given here to provide a framework for the results presented in Section 6. The FFT classification program was written for the AFGL CDC 6600 system due to computational requirements which exceeded the capabilities of McIDAS.

The classification program uses the following steps:

- (1) An $N \times N$ array of data is transformed to $N \times N$ spectral coefficients by means of a two-dimensional FFT.
- (2) The $N \times N$ spectral coefficients are summed to normalized average amplitudes (NAA) for $N/\sqrt{2}$ wavenumbers. These two steps are repeated for every case.
- (3) The NAA are sorted by cloud type and the average and standard deviation of NAA are computed for each type for all $N/\sqrt{2}$ wavenumbers.
- (4) Probabilities are computed for each cloud type.
- (5) Automatic classification is done by simply comparing the NAA for each case to the averaged NAA for each cloud type and selecting the best match. The decision is also weighted according to the a priori (dependent sample) probabilities of the cloud types.

Steps 1 through 5 are the same when either visible or IR data are used alone. When both are used together, steps 1 through 4 are run separately but the cloud type decision in 5 includes both sets of NAA.

The $N \times N$ array of data can be represented as a unique linear series of products of sines and cosines, which is a discrete two-dimensional Fourier transform. The spectral coefficients in step 1 are the coefficients of the terms in the series. Since each term in the series is associated with a particular wavelength, its coefficient is a measure of how much of the $N \times N$ data array is explained by that wavelength. For example, a data array showing one pure waveform with an integral number of waves in the array would have one spectral coefficient of unity and the rest would be zero. All of the variability of that array would be explained by one term of the Fourier transform.

In digital computer spectral analysis applications, an FFT is generally used since it reduces computer processing time and storage requirements. Other

approaches are available, including special purpose hardware and even optical devices. In our case, a FORTRAN routine by Brenner²⁰ was used. In this routine, all values of N are acceptable as array sizes. In this report, N is 37 corresponding to ground coverage of about 25 x 25 n miles. In our previous applications we used 8 and 75 as values of N. With N equal to 37, one application of the FFT subroutine to one cloud case took about 0.7 sec to run on the AFGL CDC 6600 computer and this time posed no problem for development purposes. For operational purposes, a faster and more compact program would probably be preferred. For values of N which are powers of 2, a special version of the FFT program would take about one-third as much computer storage as the unrestricted subroutine and would transform a 32 x 32 array in about 40% of the time required for a 37 x 37 array. Since complex numbers are used for both input and output, the satellite data were read in as the real parts of complex numbers and the imaginary parts were set to zero.

In step 2 of the classification program, normalized average amplitudes (NAA) are computed from the spectral coefficients. This step is significant for two reasons. First, as discussed by Sikula,¹² the number of spectral measurements is considerably reduced from N^2 to $N\sqrt{2}$ so that subsequent processing is simplified. Second, the NAA help make the classifier insensitive to the orientation of a given cloud pattern. Without NAA for example, if a pattern of cloud lines were rotated by 45 degrees, its two-dimensional transform would change considerably and an automated classifier might not assign the same cloud type to the rotated pattern.

The NAA are computed as the sums of spectral coefficients within annular bands in the frequency plane. Each band is one unit in width. The annular bands are centered on the zero order term of the FFT, which is the mean of the data array. The mean itself is the first NAA, and represents wavenumber zero. Wavenumbers assigned to the bands increase as the radii of the bands increase. The NAA are computed out to $N\sqrt{2}$, which is a Nyquist frequency for two dimensions. Aliasing occurs at wavenumbers higher than $N\sqrt{2}$ so that NAA are not computed. For an N of 37, $N\sqrt{2}$ is 26. Two variations in computing the NAA were used in this study. In one, the coefficients were summed over all quadrants of the frequency plane. This approach had been followed in earlier reports. Since it was not obvious that all quadrants were providing independent information, we tried summing the coefficients only over the first quadrant of the frequency plane. In either case, each wavenumber amplitude is averaged by dividing the number of terms entering into the sum. Results for both cases are given in Section 6.

In step 3, the NAA for all cases in an experiment are sorted by cloud type and the average and standard deviation of NAA are computed for each type for all $N\sqrt{2}$ wavenumbers.

20. Brenner, N. (1967) Special Issue on the FFT, IEEE Audio Transactions, June 1967.

In step 4, probabilities are computed for each cloud type. These are given by

$$P_i = \frac{N_i}{N_t} \quad (1)$$

with N_i the number of cases for cloud type i and N_t the total number of cases. At the completion of step 4, all the information is at hand for automated classification.

In step 5, the key parameter of the automated classification procedure is given by

$$d_i = -\frac{1}{2} \sum_{n=0}^{25} \frac{(X_n - \mu_n^i)^2}{(\sigma_n^i)^2} - \frac{1}{2} \ln \left| \sum_i \right| + \ln P_i \quad (2)$$

The index i , used as a subscript and superscript, takes the values of $i = 1, 2, 3, \dots, 9$ corresponding to the nine cloud types of Table 1. The index n refers to the wavenumbers of the NAA, X_n is an observed NAA, μ_n^i is the mean of NAA for type i and wavenumber n , σ_n^i is the standard deviation of NAA for type i and wavenumber n , P_i is the unconditional probability of type i given by Eq. (1) and

$$-\frac{1}{2} \ln \left| \sum_i \right| = \sigma_0^i \sigma_1^i \sigma_2^i \dots \sigma_{25}^i \quad (3)$$

A d_i is calculated for each of the nine cloud types for every area of satellite data read into the classification program. The decision rule selects class k if $d_k > d_i$ for all $i \neq k$. The first 26 terms of d_i measure the distance of the observed spectrum to the mean spectrum in a least squares sense. If the spectra are similar, the summation over wavenumbers yields a small negative number and d_i is likely to be chosen by the decision rule. It is important to note that the distances $(X_n - \mu_n^i)^2$ between the spectra are scaled by the variance $(\sigma_n^i)^2$. The scaling gives each wavenumber the same influence when dependent data are used in the classifier and samples are compared to their correct cloud types since

$$\sum_{j=1}^{N_i} (X_n^j - \mu_n^i)^2 : (\sigma_n^i)^2 \quad (4)$$

defines the variance for wavenumber n of type i . The index j is used for summation over the N_i cases of type i in the dependent data sample. The scaling does not insure that each wavenumber will have the same influence in rejecting a cloud type when samples are compared to incorrect cloud types. Without the scaling, the term d_i would be dominated by low wavenumbers since they have the highest NAA. This is discussed in more detail in Section 6.

The last two terms of Eq. (2) depend solely on the cloud type i and not the sample spectrum. These two terms dominate the decision process in the event that a sample spectrum is nearly the same distance from two or more mean spectra. A decision for cloud type i is favored if the next-to-last term has small standard deviations of NAA for class i . The decision is also favored if the last term represents a cloud type frequently observed in the dependent data sample.

Equation (2) is derived from a multivariate normal probability function. The probability function can be used if the class conditional probability densities for the NAA vectors are assumed as multivariate normal. A further assumption is statistical independence between the spectra of different cloud types. If these assumptions are valid, the highest value of d_i identifies the most probable cloud type.

Two forms of Eq. (2) were used in this study. It was used both with and without the last two terms in order to test the impact of the class probabilities on classification accuracy. In the selection of maximum d_i , the elimination of the last two terms is the same as if they were constant for all d_i . In other words, it is the same as assuming that all classes are equally probable.

The same computer programs were used for either visible or IR data when they were used separately for automated cloud classification. In order to use visible and IR together, the d_i computed in Eq. (2) were arbitrarily added and the maximum pair of values specified the cloud type. The decision rule selects class k if

$$d_k^V + d_k^I > d_i^V + d_i^I \text{ for all } i \neq k, \quad (5)$$

with the superscripts V and I designating visible and IR.

6. RESULTS OF THE STUDY

A number of topics are addressed in the following section. In Section 6.1, the mean spectra for nine cloud types are discussed and used to describe the strengths and weaknesses of the automated classifier. In Section 6.2, the autocorrelation of picture elements at various spatial separations is introduced and related to properties of the mean spectra. In Section 6.3, a classification using just the mean values of cloud areas is introduced as a reference to measure the performance of the automated classifier using all wavenumbers. In Section 6.4, the results of classification for all nine cloud types are presented. The various issues discussed include a comparison of classifications on two subsets of data, accuracy of classification on visible, IR, and combined data, accuracy of classification with and without

a priori probabilities of cloud types, and complete vs partial sums of Fourier coefficients to define spectra. In Section 6.5, the results for cumulus and cirrus clouds are examined in greater detail since these clouds exhibit the small-scale features which are not resolved in current automated processing. In Section 6.6, the nine categories of cloud types are combined into fewer categories so that results can be compared with the present 3DNEPH. Applications to multilayered clouds made in earlier studies are described in Section 6.7 and adjustments for varying backgrounds are discussed in Section 6.8. A possible expansion of decision equations is described in Section 6.9.

6.1 Mean Spectra of Cloud Types

Plots of mean spectra for the nine cloud types are shown in Figures 5 to 8. For clarity, four cloud types are shown in Figures 5 and 6 and the other five in Figures 7 and 8. In all subsequent discussion, the term "individual spectrum" refers to the NAA for one case while the term "mean spectra" refers to NAA averaged over all cases of a cloud type. The mean spectra in Figures 5 to 8 are from one 73-case subset of the total set of 143 cases. However, they are similar to the mean spectra for the other subset. In all cases, the spectra are scaled so that the NAA of wavenumber zero is the mean visible or IR value for the cloud type. Since the data were converted to the McIDAS 8-bit format, a value of 255 would represent the brightest possible clouds in the visible or the coldest in the IR. The mean values are considerably less than 255 since many of the $N \times N$ areas were only partly cloud covered.

All spectra are similar since the NAA are always highest at wavenumber zero and no other significant peaks appear at any other wavenumbers. The peaks at low wavenumbers were first noted by Leese and Epstein⁹ and explained as the result of gradual changes of mean cloudiness across the areas studied. In other words, there was a trend across the area. They minimized the slope of the spectra at low wavenumbers by fitting a least-squares plane to the initial data. The spectral analysis was then carried out on the residuals. Such a procedure was not followed in this study since it would minimize the difference between the means of the various cloud types and since the means are known to be useful for cloud typing. In particular, it would lead to confusion between clear areas and cloudy areas since the clear areas usually have the lowest means. The absence of significant peaks at higher wavenumbers is due to the fact that the spectra are averages of individual spectra. The individual spectra appear somewhat rougher than the averages shown here. However, the shapes and sizes of clouds vary from case to case so that the spectral peaks at high wavenumbers are more or less randomly distributed and appear smoothed out in the mean spectra.

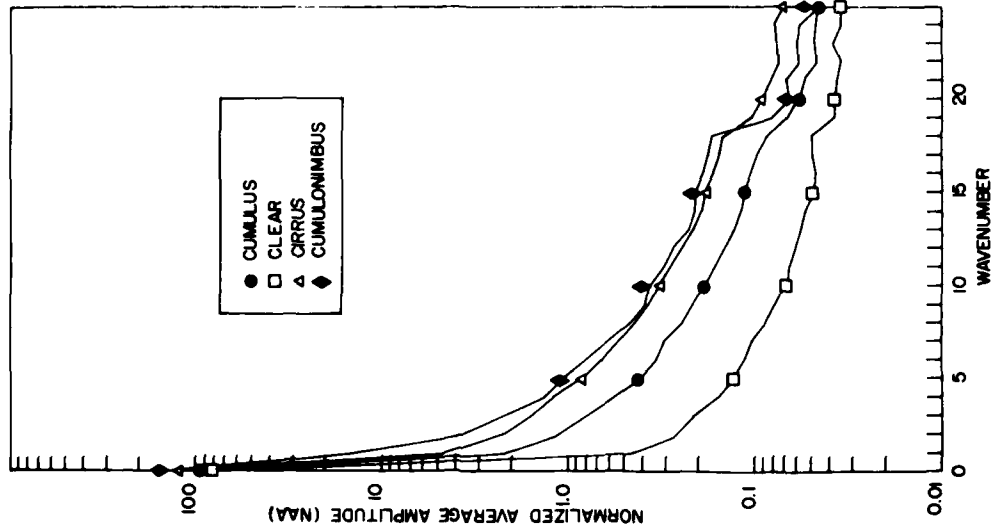


Figure 5. Mean Visible Spectra For Four of the Nine Cloud Categories of the 3DNEPH

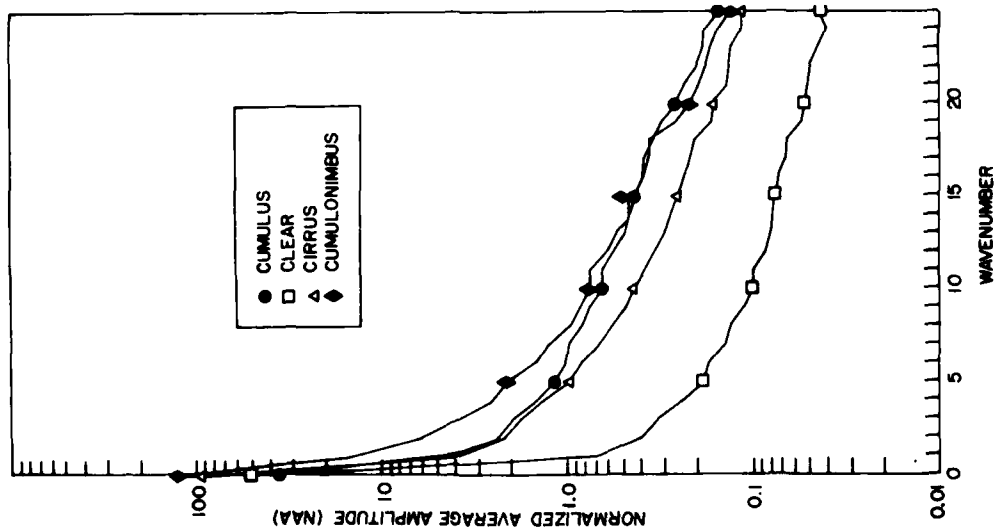


Figure 6. Mean IR Spectra For Four of the Nine Cloud Categories of the 3DNEPH

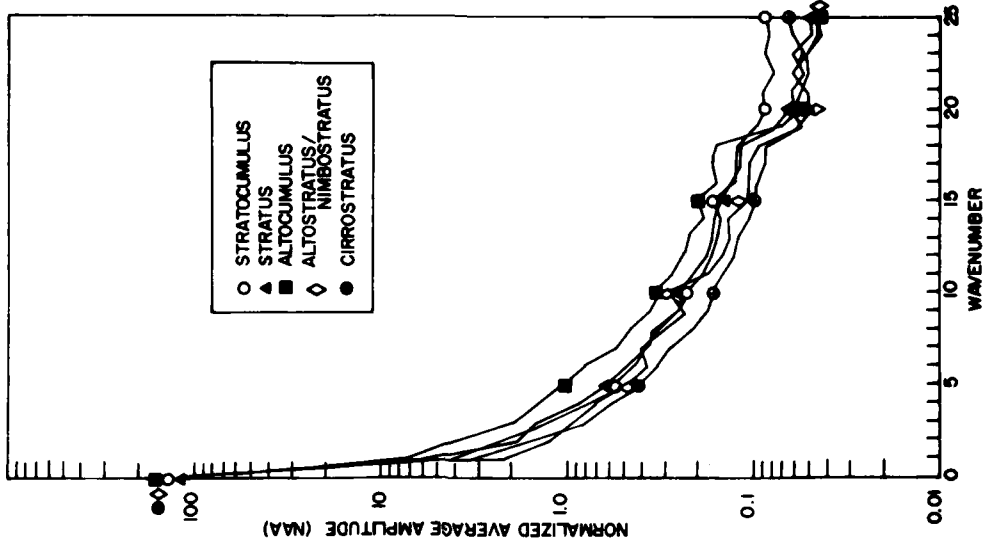


Figure 7. Mean Visible Spectra For the Remaining Five Cloud Categories of the 3DNEPH

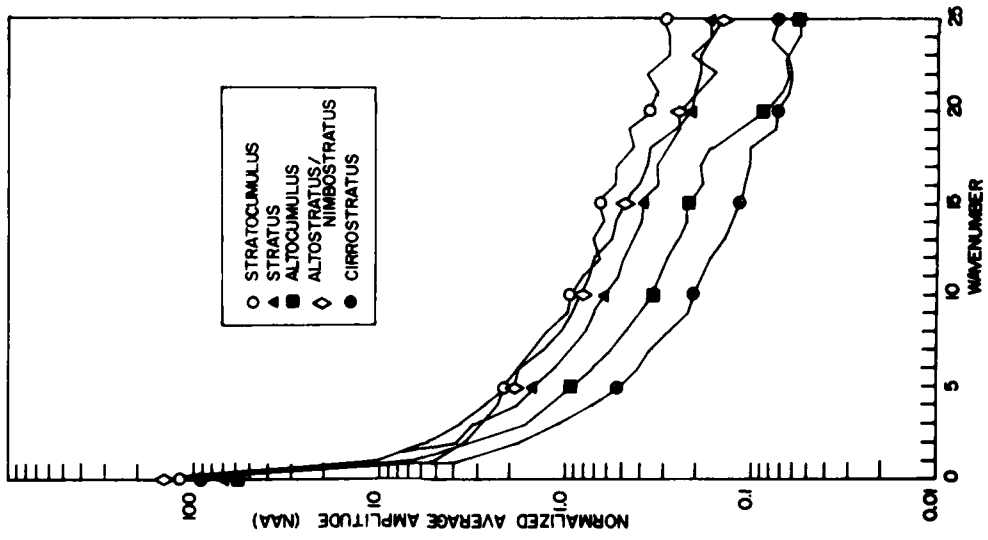


Figure 8. Mean IR Spectra for the Remaining Five Cloud Categories of the 3DNEPH

Despite the fact that the mean spectra appear somewhat similar, they are different enough for automated classification provided that an individual spectrum is closer to the mean spectrum of its type than it is to the other mean spectra. Equation (2) shows that the classifier responds only to differences in the amplitudes of spectra and is indifferent to their shapes. In Figure 5, for example, all four visible spectra have similar curvature but the spectrum for clear is low enough that it is unlikely to be confused with the others. Since all the wavenumbers are used, the spectra can be distinguished even if they overlap for some wavenumbers. Good examples of this are the visible spectra for Cu and Cb in Figure 5. They are very close at wavenumbers 10 to 24 but differ substantially at wavenumbers near zero. Another interesting feature of Figure 5 is the fact that the mean for Clear is higher than the mean for Cu since there were more clear cases over land than Cu cases over land and the land backgrounds appear fairly bright. A classifier using just the mean visible would miss the Cu while a classifier using higher wavenumbers would readily distinguish the Cu from the Clear.

Figure 6 has the mean IR spectra for the same four cloud types in Figure 5. The IR spectra have shapes similar to the visible spectra in Figure 5 but the relative position of the cloud types has changed. It was noted previously that the visible spectra for Cu and Cb were close at high wavenumbers. The IR spectra for Cu are substantially lower than the Cb spectra over the entire range of wavenumbers. The IR spectra for Cb and Ci are close at high wavenumbers but the visible spectra are not. One begins to see how the use of both visible and IR data leads to better classifications since the decision rule requires that an unknown cloudy area have both visible and IR spectra matching a particular cloud type before that type is chosen.

Two other comments regarding Figures 5 to 8 deserve mention. First, the rather smooth and featureless appearance of the average spectra suggests considerable redundancy in the information they contain. Pickett and Blackman⁶ suggested that the visible spectra they studied had about three independent pieces of information, much fewer than the number of wavenumbers used by the classifier. The second comment is that the logarithmic scale for NAA in Figures 5 to 8 is used to conveniently plot spectra for all wavenumbers and the reader should remember that the actual comparisons of spectra are scaled at each wavenumber according to the variance of NAA for each cloud type.

6.2 Autocorrelation of Picture Elements

In past applications of spectral analysis, considerable attention was given to the autocorrelation or autocovariance function. The autocorrelation function for a series of data is computed by simply shifting the series by one lag and computing the correlation coefficient between the original series and the shifted series. The

process is repeated at lags 1, 2, 3 . . . , n to give the autocorrelation to lag n. While this information is not provided by the FFT, it can be useful to help interpret the spectra.

Autocorrelation functions were generated for samples of imagery data by simply shifting the data arrays along scan lines and computing correlation coefficients for lags from 1 to 10. It was assumed that the results would be valid for variation across scan lines as well as along scan lines. Results are plotted in Figures 9 and 10 and tabulated in Tables 2a and 2b for three cases of Cb, Ci, and Cu clouds over an ocean background. The autocorrelation at lag zero is unity by definition. It remains positive for 7 lags for Cu to greater than 10 lags for Cb. The high autocorrelation for a number of lags for a short (37) series suggests that the data samples may have trends and that the spectra will show red noise or a concentration of power at low wavenumbers as was observed in the mean spectra discussed in Section 6.1. In an extreme case, the data would all lie on a plane, the autocorrelation would be unity for all lags, and the spectra would have one peak at wavenumber zero. The Cb case is the closest to this extreme.

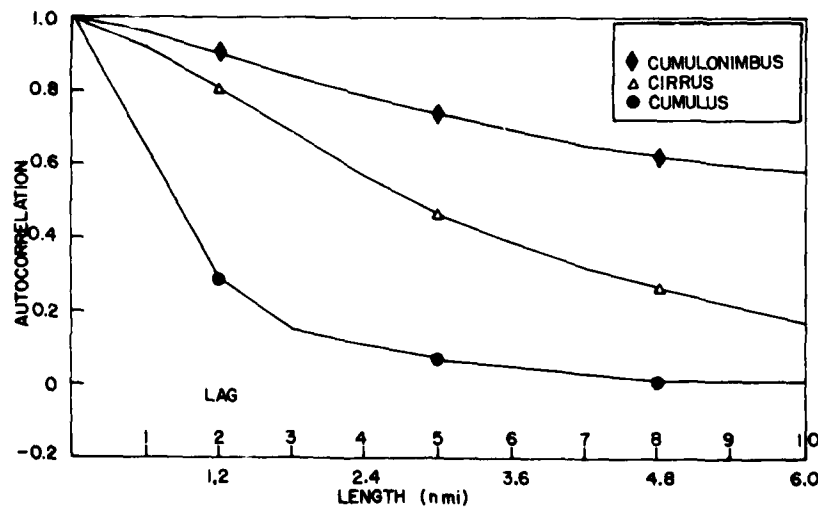


Figure 9. The Autocorrelation Function For Three Cases of Visible Data. On the abscissa, the scale for lag refers to the number of picture elements shifted while the length refers to distance (n mi) along the ground

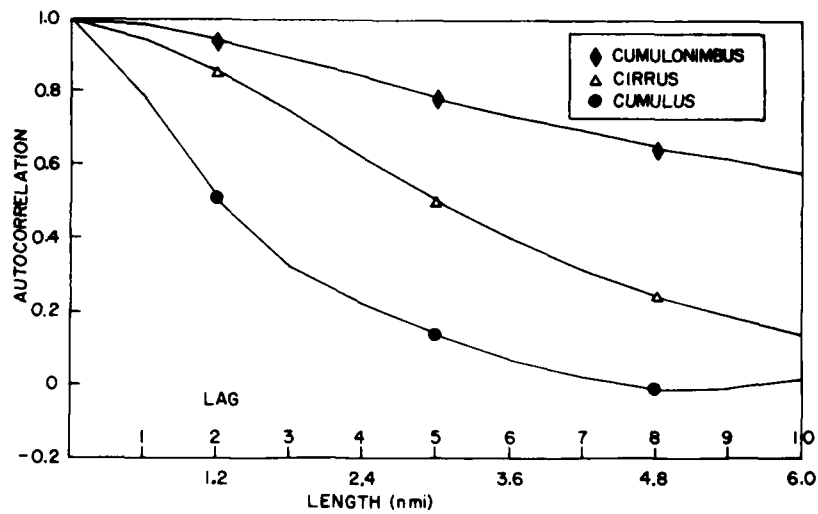


Figure 10. The Autocorrelation Function For Three Cases of IR Data

Table 2a. Autocorrelation Parameters for Visible Data. The standard errors of estimate are based on 6-bit data (values ranging from 0 to 63)

Lag	Autocorrelation			Reduction of Variance			Standard Error of Estimate		
	Cu	Ci	Cb	Cu	Ci	Cb	Cu	Ci	Cb
0	1.00	1.00	1.00	1.00	1.00	1.00	0.0	0.0	0.0
1	0.66	0.92	0.96	0.44	0.85	0.92	5.2	0.8	4.4
2	0.29	0.81	0.90	0.08	0.66	0.81	6.7	1.1	7.0
3	0.15	0.69	0.84	0.02	0.48	0.71	6.9	1.4	8.6
4	0.11	0.57	0.79	0.01	0.32	0.62	6.9	1.5	9.6
5	0.07	0.47	0.74	0.00	0.22	0.55	6.9	1.6	10.5
6	0.05	0.39	0.69	0.00	0.15	0.48	6.9	1.7	11.2
7	0.03	0.32	0.65	0.00	0.10	0.42	7.0	1.8	11.6
8	0.01	0.26	0.62	0.00	0.07	0.38	7.1	1.8	11.9
9	0.01	0.22	0.60	0.00	0.05	0.36	7.1	1.8	12.1
10	0.01	0.17	0.58	0.00	0.03	0.34	7.2	1.8	12.3

Table 2b. Autocorrelation Parameters For IR Data

Lag	Autocorrelation			Reduction of Variance			Standard Error of Estimate		
	Cu	Ci	Cb	Cu	Ci	Cb	Cu	Ci	Cb
0	1.00	1.00	1.00	1.00	1.00	1.00	0.0	0.0	0.0
1	0.79	0.94	0.98	0.62	0.88	0.96	1.3	0.8	2.2
2	0.51	0.85	0.94	0.26	0.72	0.88	1.8	1.3	3.8
3	0.32	0.74	0.89	0.10	0.55	0.79	1.9	1.6	5.1
4	0.22	0.62	0.84	0.05	0.38	0.71	2.0	1.8	6.2
5	0.14	0.50	0.78	0.02	0.25	0.61	2.0	1.9	7.0
6	0.07	0.40	0.73	0.00	0.16	0.53	2.0	2.1	7.7
7	0.02	0.31	0.69	0.00	0.10	0.48	2.1	2.1	8.2
8	-0.01	0.24	0.65	0.00	0.06	0.42	2.1	2.2	8.6
9	-0.01	0.19	0.62	0.00	0.04	0.38	2.1	2.2	8.9
10	0.01	0.13	0.58	0.00	0.02	0.34	2.1	2.2	9.2

High autocorrelation for a number of lags also suggests that the clouds and clear areas in the arrays are somewhat homogeneous so that one pixel can be used to predict the values of its neighbors. A measure of this utility is given by the reductions of variance and standard errors of estimate given in Table 2. This homogeneity of clouds and clear areas helps to minimize the impact of errors in the earth location of the data.

6.3 Classification by Mean Values

Satellite meteorologists have known for some time that the mean visible brightness or IR temperature of a cloud is useful for determining cloud type. Assuming the same fractional cloud cover, the brightest clouds tend to be Cb while the least bright clouds are usually thin Ci. High clouds such as Cs tend to appear colder than low clouds such as Sc. These properties are currently used for cloud typing in the 3DNEPH.

The cloud cases used for spectral analysis were also classified by type according to their mean visible and IR values. Since the spectral classifier uses the means as well as higher wavenumbers, it is possible to judge how much the higher wavenumbers are adding to the accuracy of classification. The mean classifier is equivalent to using only the first term of Eq. (2), that is, choose cloud type i for the minimum

$$d_i = (X_o - \mu_o^i)^2 \quad (6)$$

for visible or IR data alone. For visible and IR data together, sum the d_i for visible and IR and choose the minimum. This procedure simply finds the nearest class mean in a two-dimensional space and chooses that type. Figure 11 shows the relative positions of the computed class means. The classes which are separated the most in Figure 11 are expected to be distinguished the best by the mean classifier.

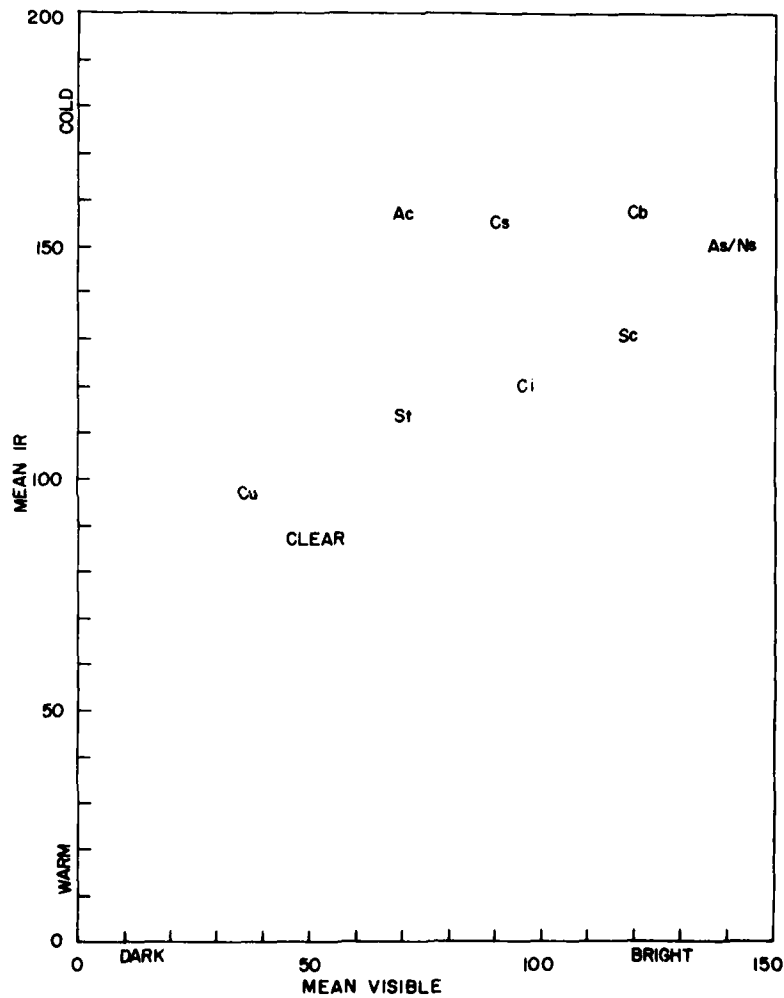


Figure 11. Mean IR and Visible Values For the Nine Cloud Categories

6.4 Classification for Nine Cloud Types

The total data set of 143 cases consists of two parts, subset 1 with 73 cases and subset 2 with 70 cases. Each subset was classified by a different satellite meteorologist. The subsets were run separately in the automatic classification program in order to see how much the program depended on the person defining the truth set. All nine cloud types were represented in each subset by two or more cases. For each subset, the classification program was run four times, that is with and without a priori probabilities of cloud types and for complete and partial sums of Fourier coefficients.

In the following discussion, it is important to note that the classification accuracies are estimated from fairly small samples of dependent data. They are likely to be less when applied to independent data or else derived from larger data samples.

A comparison of the overall performance of the classification program on the two subsets is given in Table 3, which lists the percentages of correct classifications. The performance is very nearly the same for subsets 1 and 2. The percentages given for the spectral classifier are averages for the four experiments. In the individual experiments, differences between the subsets were generally less than 7 percentage points.

Table 3. Classification Accuracy For Two Data Sets

	Visible	IR	Combined
Mean Classifier, Subset 1	34%	37%	49%
Mean Classifier, Subset 2	37%	43%	54%
Spectral Classifier, Subset 1	66%	68%	82%
Spectral Classifier, Subset 2	64%	63%	79%

The similarity in results for subsets 1 and 2 is encouraging since it suggests that the automated classification process is repeatable and not overly dependent on the person providing the cloud truth set. Moreover, since the results were so similar the remaining discussion is given for the combined results for subsets 1 and 2.

Table 4 summarizes the overall performance of the automated classifier for the nine categories listed in Table 1. In the table, the heading "1/4 coefficients" refers to the partial sums of Fourier coefficients to define NAA while the symbol θ refers to the last two terms of Eq. (2), which introduce the a priori probabilities

of cloud types. The classifications for combined visible and IR are always better than classifications for visible or IR alone. This particular result was expected since cloud types such as Ci or Sc are easily identified by meteorologists when both forms of imagery are available. Classifications for IR alone are as good as for visible alone. This result is encouraging since IR data are useful for all orbits while visible data are not useful for automated processing in dark orbits or orbits close to the terminator. The spectral classifier performs better than the mean classifier, increasing the percent correct 25 to 29 percentage points in each case. The mean classifier performs better than a random assignment of cloud types which would be expected to be correct only 1/9 or 11% of the time. On the other hand, the mean classifier is not much better than arbitrarily classifying all cases the same as the most frequently occurring cloud type. Since Ci were observed most frequently (36 out of 143 times), classifying all clouds Ci would give 25% correct.

Table 4. Classification Accuracy For Nine Categories

	Visible	IR	Combined
Means Only	36%	40%	52%
1/4 Coefficients, No θ	60%	64%	80%
1/4 Coefficients, With θ	76%	67%	82%
All Coefficients, No θ	57%	61%	81%
All Coefficients, With θ	68%	69%	79%
4-Experiment Average	65%	65%	81%

The four versions of the spectral classifier varied little in their classification accuracy. The four figures for the combined data are all within 2 percentage points of 81%. For IR alone, the figures are all within 4 percentage points of 65%. The only substantial variation is for visible data alone, where the use of a priori probabilities (with θ) gave classifications of 76 and 68% while the omission of the probabilities gave classifications of 60 and 57%. The increase in accuracy was due primarily to the improved classification of Ac.

The use of only the first quadrant (1/4 coefficients) instead of all quadrants could save a modest amount of computational time at no expense in accuracy. On the other hand, the omission of a priori probabilities of occurrence would save less computational time with a small reduction in classification accuracy.

The fact that the classifier is not sensitive to a priori probabilities was also noted by Pickett and Blackman⁶ in their application to Block 5C visible data. However, it is surprising that the occurrence probabilities are not influencing the

accuracy to a greater extent since they vary by a factor of 7 from the least probable (As/Ns) to the most probable (Ci) type. This issue was studied by examining the numerical values of terms in Eq. (2) for a number of classifications. Table 5 lists the last two terms in Eq. (2), the only terms related to the class probabilities. For a given classifier, these terms are constants depending only on the cloud type. The values given in Table 5 are for the 73 case subset with all Fourier coefficients used to define NAA. The next to last term, $-1/2 \ln \left| \frac{\bar{z}}{i} \right|$, is always larger in magnitude than the last term. The next to last term combines the standard deviations of NAA for all wavenumbers and should serve as a scaling factor for the last term. There is no obvious explanation of why it dominates unless the statistical assumptions in the derivation of Eq. (2) are not being met. One possible test which was not tried was to set the next to last term to zero or else reduce it by an arbitrary factor to see if classification accuracy would improve.

Earlier studies had suggested that a priori probabilities could be varied with location on the earth to adapt the classifier to different climates or land vs ocean influences. The present results suggest that changing the probabilities would not help the classifier unless Eq. (2) is revised.

Table 5. Numerical Values of Probability Terms for Nine Cloud Types in Subset 1

i	Visible		Infrared	
	$-1/2 \ln \left \frac{\bar{z}}{i} \right $	$\ln P_i$	$-1/2 \ln \left \frac{\bar{z}}{i} \right $	$\ln P_i$
Sc	22.843	-2.904	51.256	-2.904
St	38.670	-2.344	69.379	-2.344
Cu	38.298	-1.805	65.169	-1.805
Clear	64.967	-2.344	86.001	-2.344
Ac	74.385	-2.904	57.242	-2.904
As/Ns	47.532	-3.597	66.743	-3.597
Ci	34.182	-1.199	50.869	-1.199
Cs	55.508	-2.211	60.288	-2.211
Cb	32.404	-2.344	54.892	-2.344

6.5 Detection of Small-Scale Cloud Features

The overall accuracy of classification for nine cloud categories is not the only measure of merit for automated classification of fine mode data. An equally important consideration is how well it detects small-scale cloud features that are

poorly resolved by smoothed mode data in the current nephanalysis. Among lower clouds, cumulus clouds tend to have the smallest sizes and at times they are not detected in smoothed mode data. For high clouds, cirrus tends to have the smallest or least distinguishable cloud features. Results for Cu are given in Table 6. Cumulus clouds were correctly chosen 66% of the time, misclassified as another cumuliform (Cb, Sc or Ac) 21% of the time, and misclassified as hightypes (Cs or Ci) 12% of the time using visible data. Significantly, in no cases were Cu undetected, that is, misclassified as clear areas. They are either classified correctly or as some other cloud type. The IR classifier did not do as well (55% to 66%) but it mislabeled Cu cases as clear only 1% of the time. Regarding cirrus, the IR classifier was successful 72% of the time and never mislabeled a Ci case as clear. Visible data were less reliable for cirrus detection (50% compared to 72%). The combined classifier did well for both Cu (77%) and Ci (76%) and never misclassified them as clear.

Table 6. A Comparison of Observed Cloud Types to Automated Classifications. The numbers tabulated are percentages of the observed cases. Some columns do not sum to 100% due to rounding off to the nearest percent

Automated Classification	Observed Type					
	Visible		IR		Combined	
	Cu	Ci	Cu	Ci	Cu	Ci
Sc	7	8	19	9	5	6
St	0	6	1	3	2	2
Cu	66	0	55	6	77	3
Ac	5	1	2	0	3	0
As/Ns	0	0	0	0	0	0
Ci	10	50	15	72	2	76
Cs	2	15	7	3	4	8
Cb	9	8	0	7	6	6
Clear	0	13	1	0	0	0

6.6 Comparison to 3DNEPH

Appendix I of the 3DNEPH report by Fye¹ describes an empirical determination of cloud types from IR and visual satellite imagery. The 3DNEPH types clouds using an empirical set of weighted equations and thresholds which are functions of visual and IR grayshade and variability. The 3DNEPH report does not give an

exact definition of "grayshade" and "variability" as used by the cloud typing routine nor does the report indicate the extent to which the cloud typing depends on the visual and IR data processors, which provide considerable information for cloud detection and estimates of the horizontal and vertical coverage of cloud layers. Nephanalysis specialists at AFGWC defined G , the visual grayshade, as the average of visible data over an eighth-mesh box (about 25×25 n mi) and the visual variability as

$$V = N^{-1} \sum_{i=1}^N |G_i - \bar{G}| \quad (7)$$

where G_i is a visible datum and N is the total number of data elements. The average \bar{G} is the same as the mean value used in the mean classifier and the spectral classifiers discussed in Sections 6.3 and 6.4. The variability V , which is sometimes called the mean deviation, is not the same as any of the wavenumbers used by the spectral classifiers.

The IR grayshades and variabilities used for cloud typing have been defined in several ways since cloud typing originated in 1976. Early routines used the same definitions of means and variabilities for both IR and visible data. More recently, surface temperatures, independent of the satellite IR temperatures, are used as a reference for the IR grayshade.

When both visible and IR data are available, cloud typing is done for the eight cloud categories in Table 1. The category clear is not assigned. If only visible data are available, only Cb clouds are typed. If only IR data are available, low clouds are excluded and only the middle and high clouds are typed. The four categories for IR typing are (As/Ns), Ac, (Cs/Cb), and Ci. The two types Cs and Cb are merged into a supercategory for purposes of comparison with the results of this report following the advice of AWS technical personnel, who pointed out that Cs and Cb are difficult to distinguish in the 3DNEPH IR cloud typing.

The accuracy of 3DNEPH cloud typing was found to be 80% in development tests. A verification program (CLOVER) found surface reports closely timed to satellite data indicating only one cloud type. The program used IR data to check for cloud layers which might be hidden from the observers and removed these cases from the verification.

The results presented in Section 6.4 were retabulated for comparison to the 3DNEPH categories and are given in Table 7. For combined visible and IR data, the average performance of the spectral classifier dropped from 81% to 80%. The clear category, which was purged, had a classification accuracy of 85% so that results for eight categories are less than for nine categories. For visible data alone, 82% of Cb clouds were typed correctly. For IR data alone, 70% of middle and high

cloud cases were typed correctly. The bracketed numbers in Table 7 give the increase in accuracy due to merging Cs and Cb cases into a supercategory in the IR classifiers. The increases are very small (1 or 2 percentage points) for the spectral classifiers indicating that the spectral classifiers, unlike the 3DNEPH, rarely confuse Cs and Cb clouds.

Table 7. Classification Accuracy For 3DNEPH Categories

Eight Categories (No Clear Cases)			
	Visible	IR	Combined
Means Only	35%	35%	51%
1/4 Coefficients, No θ	58%	62%	81%
1/4 Coefficients, With θ	73%	63%	81%
All Coefficients, No θ	54%	59%	82%
All Coefficients, With θ	64%	66%	77%
4-Experiment Average	62%	62%	80%
One Category (Cb only)			
	Visible		
Means Only	29%		
1/4 Coefficients, No θ	86%		
1/4 Coefficients, With θ	86%		
All Coefficients, No θ	79%		
All Coefficients, With θ	79%		
4-Experiment Average	82%		
Four Categories (As/Ns), Ac, Ci, (Cs/Cb)			
	IR		
Means Only	43%	(+13)	
1/4 Coefficients, No θ	69%	(+1)	
1/4 Coefficients, With θ	70%	(+1)	
All Coefficients, No θ	69%	(+1)	
All Coefficients, With θ	73%	(+2)	
4-Experiment Average	70%	(+1)	

The accuracies of the spectral classifier (80% for visible and IR, eight categories; 82% for visible, one category; 70% for IR, four categories) are about the same as the 80% figure given for development tests of the 3DNEPH.¹ Since our study and the 3DNEPH used different data sets and different methods to select cloud cases to verify the classifiers it is not possible to judge which approach works best. If both classifiers were used on the same data, we expect the spectral classifier would perform as well as or better than the 3DNEPH classifier since the spectral classifier uses the mean and 25 wavenumber parameters while the 3DNEPH uses the mean and only one other parameter, the variability.

The spectral classifiers were substantially more accurate than the mean classifiers, for example 70% accuracy was found for four categories in IR data instead of 43% for the mean classifier. The increased accuracy is due to the 25 wavenumber parameters in the spectral classifier. For the 3DNEPH classifier, we do not know how much of the classification accuracy is due to the means and how much is due to the variabilities. This information, if known, would be very helpful for evaluating the utility of wavenumber parameters since it would show how much classification accuracy was due to the carefully tuned but simply defined statistic of variability.

6.7 Multilayered Clouds and Merged Categories

A multilayered category was not included in our study since we used the 3DNEPH categories given in Table 1 and concentrated on the categories cumulus and cirrus which exhibit small-scale features. In a global application, however, multilayered clouds would be encountered and the spectral classifiers discussed in this report would assign some single cloud category to these areas. Although we did not test mixed cases, it is our opinion that a multilayered scene such as Ci over lower cloud would be assigned a high cloud type such as Ci or Cb by the IR or combined spectral classifiers. It is less clear what the visible classifier would do with multilayered clouds.

The studies summarized in Table 8 were able to detect multilayered clouds with some skill but there was a difference of opinion as to how well it was done. Booth¹¹ and Parikh¹⁴ used a multilayered category described as Ci + low. This category included all cases of cirrus above middle clouds or low clouds. Booth's¹¹ results show that the Ci + low classification accuracy was about the same as the overall classification accuracy and he maintained the Ci + low category in all his experiments. Using SMS-1 data, Parikh¹⁴ concluded that the multilayer class was not well separated from the other classes and that classification accuracies could be improved by removing the multilayered class.

Table 8. Cloud Categories Used in Cloud Classification Studies

Number	Booth ¹¹	Booth ¹¹	Parikh ¹⁴	Parikh ¹⁴	Harris and Barrett ¹⁵
1	Clear	Clear	Cu/Sc/St	Cu/Sc/St	Clear
2	Cu	Cu/Sc/St	Ci + low	Ci	Stratiform
3	Sc/St	Cb	Ci	Cb	Cumuliform
4	Cb	Ci	Cb		Stratocumuliform
5	Ci	Ci + low			
6	Ci + low				
Classification Accuracy					
Visible	43-54%	44-55%			72%
IR	57-60%	63-70%			75%
Combined	63-76%	69-81%	81-89%	90-96%	

All of the studies in Table 8 used fewer categories than we used by merging categories like Sc and Cu into supercategories such as (Sc/Cu). The use of supercategories improves the overall classification since misclassifications to closely related categories are counted as hits rather than misses. The increase in classification accuracy by the use of supercategories tends to offset the decrease in accuracy which may occur if a multilayered category is introduced.

The approach to classification followed in this report could be modified to be similar to the other studies. A condensed version of the categories in Table 1 is presented in Table 9. All low clouds are merged into one category (St/St/Cu), all middle clouds are merged into one category (Ac/As/Ns), cirrus is combined with cirrostratus (Ci/Cs), while cumulonimbus and clear are kept as separate categories. Classification accuracies are high (73% for visible, 72% for IR, 86% for combined) and the inclusion of a multilayered class might not degrade the classification accuracies to an unacceptable level.

6.8 Adjustments for Varying Backgrounds

The variability of backgrounds encountered in a global application of cloud typing algorithms is of particular concern. Extreme backgrounds may appear so bright in the visible or so cold in the IR that no technique can detect clouds over these backgrounds with confidence. For visible data, an example of an extreme background would be an ice cap or tundra covered by fresh snow. For IR data, in addition to the very cold temperatures observed near the South Pole there are parts of Siberia with monthly mean temperatures below -50°C.

Table 9. Classification Accuracy For Five Categories (Sc/St/Cu), (Ac/As/Ns), (Ci/Cs), Cb, Clear

	Visible	IR	Combined
Means Only	44%	48%	59%
1/4 Coefficients, No θ	67%	69%	83%
1/4 Coefficients, With θ	81%	75%	89%
All Coefficients, No θ	66%	67%	84%
All Coefficients, With θ	76%	77%	86%
4-Experiment Average	73%	72%	86%

Between the well-behaved backgrounds, which were generally used in the studies cited, and the extreme backgrounds, which no one used, there remains a great range of background conditions encountered while sensing clouds from satellites. In the 3DNEPH, the great range of conditions is handled by comparing the visible data to background brightness fields and the IR data to clear column temperature fields derived from surface and sounding data or forecast models. The preparation of background fields probably requires as much data processing as any other part of the 3DNEPH. The experience gained in developing background fields for the 3DNEPH suggests that the development of similar background fields for a spectral classifier would be a lengthy and computationally intensive process.

The 3DNEPH approach to background fields could be extended to the spectral classifiers. For visible data, mean spectra for the category of clear could be derived for all locations on the earth. The clear spectra would look different, depending on whether the background was land, ocean, snow, or some mixture. The individual spectrum for an unknown case could be classified by comparing it to the location-dependent clear spectrum as well as the mean spectra for cloud categories. Cloud categories with mean spectra nearly the same as the clear spectrum could be earmarked as undetectable at that location. Snow covered areas, which tend to be the brightest backgrounds, would probably be the most difficult backgrounds for spectral classifiers as they are for the first order statistics in the 3DNEPH.

The 3DNEPH does not handle the background fields for IR data in the same way that it does for visible data. Since clear column temperatures will vary from day to day for a given location, a reference field is prepared which is independent of the satellite data. The reference field, which is a short term forecast based on surface and sounding temperatures, is rather coarse compared to the satellite data. Only a mean clear column temperature can be derived for a 25×25 n mi area. The higher wavenumbers cannot be directly derived. It may be possible to scale

the mean spectra for the clear category based on the mean clear column temperature anticipated at a given location, but some experimentation would be required. In the absence of special enhancements, it is harder to see surface features in the IR data due to attenuation of the surface radiation by water vapor and other gases. Important exceptions are coastlines with a strong temperature gradient from water to land. The relatively uniform appearance of most clear areas in the IR data suggests that the high wavenumbers of the spectrum will not vary much from case to case, so that scaled reference spectra based on a mean temperature may be adequate for the clear category.

6.9 Visible and IR Covariance Consideration

One experiment suggested by Pickett and Blackman⁶ has not been done. When combined visible and IR data are available, we analyze them separately until the final step of the cloud typing decision. This means that the visible and IR images are never compared on a pixel by pixel basis. Pickett and Blackman⁶ suggested that covariances of visible and IR could be added to the decision equations. Presently, we use 26 NAA for visible and 26 for IR. Adding the covariance information would add 26 terms to the decision equations. Adding these terms should help to distinguish Cb cases from Cs cases and also Cu cases from clear cases since the Cb or Cu cases have highly correlated visible and IR images while the Cs and clear cases do not. The improvement in classification accuracies might be small, however, since spectral classifiers for visible and IR data combined are already doing a good job of distinguishing Cb cases from Cs and Cu cases from clear.

7. CONCLUSIONS

We are encouraged that small-scale cloud features exemplified by cumulus or cirrus clouds are observed as high amplitudes at high wavenumbers of the two-dimensional FFT applied to time made visible and IR imagery data. The high amplitudes lead to good classifications by the spectral classifier (77% for Cu and 76% for Ci for visible and IR data combined). The classification accuracies for the spectral classifier were substantially better than for the mean classifier. Most of the misclassifications gave closely related cloud types such as Sc instead of Cu. It is particularly significant that the small-scale clouds, Cu and Ci, were not misclassified as clear areas. Also Cu cases were successfully detected by the visible spectral classifiers over both bright and dark (land and ocean) backgrounds as long as the backgrounds appeared uniform and did not contain coastlines or snowcover.

The classification accuracies for all cloud categories, including large as well as small cloud features, were not significantly better than accuracies observed in

other studies which used coarser resolution satellite data and did not rely on transform statistics. One explanation of why the transform statistics did not do better is that the two-dimensional FFT is sensitive to the sizes and shapes of clouds, but the sizes and shapes are never quite the same from case to case. The cloud patterns we observed were like fingerprints, since the images were often similar but no two cases were identical. The differences in the images lead to substantial variation from spectrum to spectrum for a given category. Another explanation for misclassifications by the spectral classifiers is that even if the cloud elements for a category had the same size and shape for every case, the cloud elements might not be distributed over the entire area of analysis. For example, if a Cb anvil covers an entire area, its spectrum will not look the same as the spectrum that would be found if the area of analysis were shifted so that the Cb anvil covered only a part of the area. The problem is essentially the variability of horizontal cloud cover from case to case. It is easy to see how the variability of horizontal cloud cover limits the mean classifiers. We also believe that changes in cloud cover for a given category produce changes in all the wavenumbers of the spectrum and are a source of confusion for the spectral classifiers as well. This problem could be studied further by classifying specially designed test patterns or else partially overlapping areas of real data. It might also be possible to improve the spectral classifiers by introducing estimates of fractional cloud cover. One possibility would be to use an estimate of fractional cloud cover to scale an individual spectrum to some standard fractional cover before comparing it to the mean spectra.

The comparison of classification accuracies found in this study to accuracies observed by the 3DNEPH is complicated by the use of different data samples and verification procedures. It would be much better to repeat the classifications we described along with the 3DNEPH analysis in order to see what improvements are evident when both approaches are followed on the same data sample. The first order statistics used in the 3DNEPH on smoothed-mode satellite imagery could also be used on fine mode imagery as a fairer test of the spectral classifiers, which use fine mode imagery. These comparisons could also consider various options for spectral classification, such as whether or not to include a priori probabilities or the use of complete vs partial sums of coefficients to define NAA.

The procedures that we and other investigators have used to label cloud cases in order to train automated classifiers are somewhat limited. Even with the help of an interactive system like the McIDAS, it does take time to find an adequate distribution of cases. Also, meteorologists who label the cloud cases have difficulty finding some cases such as middle clouds or distinguishing between categories such as Cb and a dense Cs. In other words, the meteorologists experience indecision in a manner similar to the automated classifiers. These limitations suggest that neither cloud truth sets nor the automated classifiers derived from them will

ever approach 100% accuracy unless the present methods for building cloud truth sets can be improved. One possibility would be to abandon descriptive cloud categories such as cumulus or stratocumulus and work with measured quantities such as the average size of clouds in a predefined area.

The work which has been done can be viewed in perspective if we review the fourteen recommendations for future investigations proposed by Sikula¹² in 1974. Much work has been done and most of his recommendations have been studied by someone. For examples, very high resolution infrared radiances have been used as input to the FFT and grid sizes other than 25 n mi have been used. Two tough questions remain, however. One question is how to remove the effect of the backgrounds from the computed NAA and the other question is how to best combine other statistics such as modes from the existing IR processor or estimates of fractional cloud amounts with the computed NAA. These questions of backgrounds and the optimum mix of transform statistics with first order statistics need to be answered before applications of FFTs to global satellite data can offer significant improvements to cloud analysis.

References

1. Fye, F.K. (1978) The AFGWC Automated Cloud Analysis Model, AFGWC Technical Memorandum 78-002.
2. Coburn, A.R. (1971) Improved Three-Dimensional Nephanalysis, AFGWC Technical Memorandum 71-2.
3. Pickett, R.M., and Blackman, E.S. (1976) Automated Processing of Satellite Imagery Data at Air Force Global Weather Central, BBN No. 3275, Interim Report. FI9628-76-C-0124, Bolt Beranek and Newman Inc., Cambridge, MA 02138.
4. Blackman, E.S., and Pickett, R.M. (1977) Automated Processing of Satellite Imagery Data at the Air Force Global Weather Central: Demonstrations of Spectral Analysis, AFGL-TR-77-0080, AD A039918.
5. Fournier, R.F. (1977) An Initial Study of Power Spectra for Satellite Imagery, AFGL-TR-77-0295, AD A058483.
6. Pickett, R.M., and Blackman, E.S. (1979) Automated Processing of Satellite Imagery Data: Test of a Spectral Classifier, AFGL-TR-79-0040, AD A068663.
7. Hawkins, R.S. (1977) A New Automatic Processing Technique for Satellite Imagery Analysis, AFGL-TR-77-0174, AD A049350.
8. d'Entremont, R. (1980) Performance of the Discrete Fourier Transform Satellite Imagery Classification Technique, Tech. Rept. Submitted to AFGL under Contract FI9628-79-C-0033.
9. Leese, J.A., and Epstein, E.S. (1963) Application of two-dimensional spectral analysis to the quantification of satellite cloud photographs, J. Appl. Meteor. 2:629-644.
10. Darling, E.M., and Joseph, R.D. (1968) Pattern recognition from satellite altitudes, IEEE Trans. on System Science and Cybernetics, SSC-4(No. 1):38-47.
11. Booth, A.L. (1973) Objective cloud type classification using visual and infrared satellite data in Proceedings of the 3rd Conf. on Probability and Statistics in Atmospheric Science, American Meteorological Society, Boston, MA 02108, pp 220-227.

References

12. Sikula, G. J. (1974) Spectral signatures of several cloud types and information extraction from very high resolution visual satellite radiances-preliminary results in Paper for 6th Conf. on Aerospace and Aeronautical Meteor., El Paso, TX.
13. Parikh, J. (1977) A comparative study of cloud classification techniques, Remote Sensing of Env. 6:67-81.
14. Parikh, J. (1978) Cloud classification from visible and infrared SMS-1 data, Remote Sensing of Env. 7:85-92.
15. Harris, R., and Barrett, E. C. (1978) Toward an objective nephanalysis, J. Appl. Meteor. 17:1258-1266.
16. Steiner, D., and Salerno, A. E. (1975) Remote sensor data systems, processing and management, Manual of Remote Sensing, Keuffel and Esser Co., pp 611-803.
17. Duda, R. O., and Hart, P. E. (1973) Pattern Classification and Scene Analysis, John Wiley and Sons.
18. Nichols, D. A. (1975) Block 5D Compilation, Defense Meteorological Satellite Program, Los Angeles AFS CA 90009.
19. Spangler, M. J. (1974) The DMSP primary data sensor in Proceedings of the 6th Conf. on Aerospace and Aeronautical Meteor. El Paso, TX, pp 150-157.
20. Brenner, N. (1967) Special Issue on the FFT, IEEE Audio Transactions, June 1967.

Appendix A

Implications of Changing the Resolution of Satellite Data

All of the results presented in this report are based on a special data sample with 0.6 n mi ground resolution for each data element. This special sample led to an FFT array size of 37×37 to match the 25×25 n mi boxes of the 3DNEPH. In future applications, 0.3 n mi data could be used and the following options are available for analysis over the standard areas of 25×25 n mi:

- (1) Do the same thing. Smooth data to 0.6 n mi and use an array of 37×37 for the FFT,
- (2) Apply the same computer program to four 37×37 subarrays of 0.3 n mi data,
- (3) Reprogram to a larger array (about 75×75 of 0.3 n mi data,
- (4) Reprogram to array sizes (such as 32×32 or 64×64) which are powers of two.

Options (1) and (2) have the advantage of requiring no reprogramming effort. The use of 0.3 n mi data in options (2) and (3) should provide the best detection of small-scale cloud features. Option (3) would require the most computer time since the array is large and the dimension is not a power of two. Option (4) would not exactly cover a 25×25 n mi area due to the restriction to powers of two but it should provide the fastest computer time. Some experimentation would be required to choose the best option and a development sample considerably larger than

our 143 cases should be used to make the decision. The use of four smaller arrays is equivalent to decreasing the mesh size for cloud typing. This option was suggested by observations that relatively few wavenumbers contribute independent information to the spectral classifiers.

